Differential polarization imaging

V. Numerical aperture effects and the contribution of preferential scattering and absorption to the circular dichroism images

Laura Finzi, Laura Ulibarri, and Carlos Bustamante
Department of Chemistry, The University of New Mexico, Albuquerque, New Mexico 87131 USA

ABSTRACT Chiral objects which scatter and absorb preferentially left versus right circularly polarized light give rise to bright-field circular dichroism (CD) images containing contributions from both these two phenomena. These contributions are separated and characterized mathematically, and the effect of the dimensions of the chiral object on their relative magnitude is discussed. CD images of the long-range chiral organization of the thylakoid membranes in chloroplasts are obtained at two different wavelengths to illustrate the diverse wavelength dependence of the preferential absorption and scattering contributions to the images. The bright field CD images not only depend on the magnitude and sign of the preferential scattering and preferential absorption contributions, but also on the numerical aperture of the lens used. This dependence is obtained formally and a method to extract the angle dependent preferential scattering contributions to the images is presented. The validity of this method is confirmed experimentally.

I. INTRODUCTION

Biological systems are frequently organized in hierarchical chiral structures, often revealed by the strong and complex optical activity signals displayed by these systems. In particular, the circular dichroism (CD) spectra of these samples are characterized not only by signals due to preferential absorption of right versus left circularly polarized light, but also by signals due to the preferential scattering of these two circular polarizations. The latter are displayed by chirally organized macroaggregates having dimensions commensurate to the wavelength of the light, and appear as tails outside the absorption band, where the differential absorption vanishes. This phenomenon has been termed circular intensity differential scattering (CIDS) (1) and its contribution to the appearance of the CD spectrum depends on the size of the collected cone of light. This was first recognized by Dorman et al. (2) and Bustamante et al. (3).

Preferential absorption and CIDS can contribute also to the circular dichroism (M_{14} entry of the Mueller matrix) images of biological structures possessing a long-chiral organization (4) (see also accompanying paper). The preferential power loss away from the forward direction due to the preferential scattering mechanism, or CIDS, gives rise, in bright field geometry, to an "apparent" circular dichroism contribution to the image which will be referred to as CD^{sca}, to differentiate it from the differential absorption contribution (CD^{abs}). Thus, the M_{14} image of an object that can both *absorb* and *scatter* preferentially one of the circular polarizations over the other is the sum of the two contributions due to CD^{abs} and the CD^{sca} and it will be referred to as the observed CD image of the object (CD^{obs}):

$$CD^{obs} = CD^{abs} + CD^{sca}. \qquad (1)$$

Section II A of this paper shows how to separate theoretically the absorption from the scattering contribution to the M_{14} image. In section II B the effect of the numerical aperture of the lens on the M_{14} image is derived. It will be shown that the comparison of M_{14} images taken with lenses of different numerical apertures permits isolation and characterization of the scattering occurring in the cone delimited by the acceptance angles of the two lenses. Section III contains two different types of numerical computations. The absorption and scattering contributions to the M_{14} image of different size model helices are presented in section III A. Section III B includes numerical computations on the effect of the numerical aperture of the lens on the M_{14} image. The experimental confirmation on the lens dimension effect on the M_{14} image of a biological sample will be presented in section IV. In this section CD images of chloroplasts, obtained at the center and outside the absorption band of the chromophores, are used to evidentiate the absorption and scattering contribution to these images.

Address correspondence to Dr. Carlos Bustamante.

0006-3495/91/06/1183/11 $2.00

II. THEORY

A. Separation of the absorption and scattering contributions to the M_{14} images

It was shown in section III A of the previous paper (4b) that the M_{14} and M_{41} bright field Mueller images are sensitive to the chiral nature of the object. Their expressions are given by (see Eqs. 13 and 14 of the previous paper [4b]):

$$\begin{aligned} M_{14} &= -iA[B(\underset{\sim}{1} \times \mathbf{F}^{\dagger} - \mathbf{F} \times \underset{\sim}{1})_{\alpha\beta\gamma} \\ &\quad + (\mathbf{F} \times \mathbf{F}^{\dagger})_{\alpha\beta\gamma}](\underset{\sim}{1} - \hat{\mathbf{z}}\hat{\mathbf{z}})_{\alpha\gamma}\hat{\mathbf{z}}_{\beta} \\ M_{41} &= iA[B(\underset{\sim}{1} \times \mathbf{F} - \mathbf{F}^{\dagger} \times \underset{\sim}{1})_{\alpha\beta\gamma} \\ &\quad + (\mathbf{F}^{\dagger} \times \mathbf{F})_{\alpha\beta\gamma}](\underset{\sim}{1} - \hat{\mathbf{z}}\hat{\mathbf{z}})_{\alpha\gamma}\hat{\mathbf{z}}_{\beta}, \end{aligned} \tag{2}$$

where A and B are constants, whose exact values can be found in paper I of this series (5), and $\hat{\mathbf{z}}$ is a unit vector in the direction of propagation of the incident light. It was also shown that the form of the tensor $\mathbf{F}$ appearing in Eq. 1, depends on whether or not the treatment describes the interaction among the polarizable groups in the object. In the first Born approximation, $\mathbf{F}$ is given by:

$$\mathbf{F}_{1st} = \frac{J_1\left(\frac{ka\rho_i}{r}\right)}{\frac{ka\rho_i}{r}} \boldsymbol{\alpha}_i, \tag{3}$$

where $\boldsymbol{\alpha}_i$ is the polarizability tensor of group i, $J_1(ka\rho_i/r)$ is a bessel function of the first kind of order one, $k = 2\pi/\lambda$, a is the radius of the lens, λ is the wavelength of the light, and $\rho_i = \sqrt{(x + mx_i)^2 + (y + my_i)^2}$. In the definition of ρ_i, x, and y are the Cartesian coordinates of $\mathbf{r}$, the vector pointing from the center of the lens to the image point on the detector screen, whereas x_i and y_i are the Cartesian coordinates of $\mathbf{r}_i$, the vector of the ith polarizable group in the object, and m is the magnification of the imaging system (refer to Fig. 1 of paper I [5] for details). In the second Born approximation, $\mathbf{F}$ becomes:

$$\mathbf{F}_{2nd} = \sum_{i}^{N} \frac{J_i\left(\frac{ka\rho_i}{r}\right)}{\frac{ka\rho_i}{r}} \boldsymbol{\alpha}_i \cdot (\underset{\sim}{1} + 4\pi k^2 \sum_{j \neq i} \boldsymbol{\Gamma}_{ij} \cdot \boldsymbol{\alpha}_j \cdot e^{i\mathbf{k}_0 \cdot \mathbf{r}_{ij}}), \tag{4}$$

where $\boldsymbol{\Gamma}_{ij}$ is the dipole interaction tensor between groups i and j in the object.

In the following discussion, attention will be focused on the M_{14} entry of the Mueller matrix, which represents the circular dichroism of the object. If the group polarizabilities are real and symmetric, the two terms inside the square bracket in Eq. 2 vanish in the first Born approximation, but not necessarily in higher Born approximations where interactions between the polarizable groups are included. The second term in the bracket, $(\mathbf{F} \times \mathbf{F}^{\dagger})$, describes the circular intensity differential scattering (CIDS) of the object in the forward direction. This term is proportional to the second power of the group polarizabilities and can be neglected relative to the first term, $(\mathbf{1} \times \mathbf{F}^{\dagger} - \mathbf{F} \times \mathbf{1})$. This latter term describes the "shadow" contribution to the bright field M_{14} image due to the ability of the chiral object to remove the energy differentially between the incident right and left circularly polarized light. Therefore, this term is proportional to the observed circular dichroism (CD^{obs}) image of the sample; it contains the contribution of the preferential absorption of the object, or CD^{abs} and the contribution of the preferential scattering away from the forward direction (CD^{sca}).

Fig. 1, *a* and *b*, show a diagram depicting the two mechanisms that can give rise to a CD^{obs} image. The preferential scattering is depicted in Fig. 1 *a* in the form of a CIDS pattern,

$$\left(\mathrm{CIDS} = \frac{I_{\mathrm{L}}^{sca} - I_{\mathrm{R}}^{sca}}{I_{\mathrm{L}}^{sca} + I_{\mathrm{R}}^{sca}}\right),$$

where $I_{\mathrm{L,R}}^{sca}$ is the intensity scattered in a given direction by the chiral object when it is illuminated by left-(L) or right-(R) circularly polarized incident light. The CIDS pattern shows the characteristic scattering lobes of alternating signs as a function of the scattering angle (1).

It is of interest to separate the two contributions to the $(\mathbf{1} \times \mathbf{F}^{\dagger} - \underset{\sim}{\mathbf{F}} \times 1)$ in Eq. 2, because they do not necessarily contribute to CD^{obs} in the same way. In fact, the magnitude and sign of the two contributions is a function of the chiral dimensions of the object. In particular, preferential scattering is an indication of long-range chirality; groups far apart in the object, maintaining a chiral relationship with each other contribute more to the preferential scattering than groups separated by distances much shorter than the wavelength of light. On the other hand, the preferential absorption part of the signal can have long- and short-range origins.

The separation of CD^{abs} and CD^{sca} can be done according to the following procedure. First, an M_{14} image of the object is obtained using a wavelength (λ_{in}) within the absorption band of the chromophores in the object. This image contains absorption and scattering contributions (CD^{obs} image). Then a second M_{14} image is obtained using a wavelength of light falling outside the absorption band (λ_{out}). The image so obtained will contain only the contribution of CD^{sca}. The CD^{abs} image

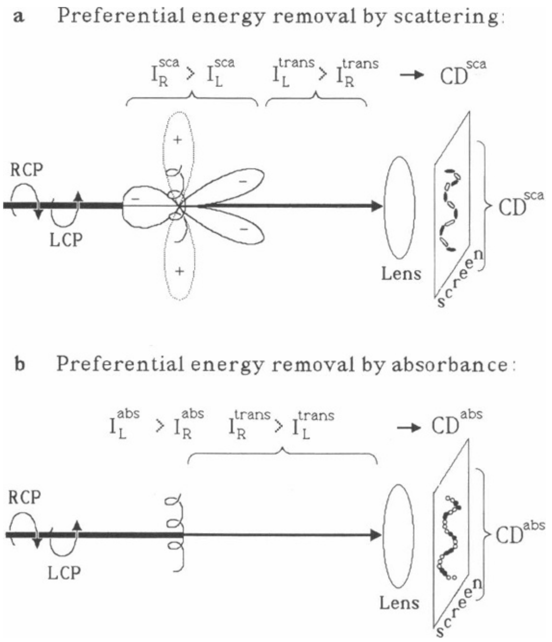

FIGURE 1 The two possible contributions to the M_{14} image of a right-handed helix are diagrammed. Light of alternating circular polarizations impinges on the helix and it is preferentially scattered (*a*) and/or absorbed (*b*). The preferential scattering is depicted by the characteristic lobes of alternating sign. Because overall, one of the two circular polarizations is scattered more than the other, this last one will be predominant in the transmitted beam in the forward direction. This gives rise to an apparent CD (see image of the helix on the detector screen of *a*). On the other hand, the helix may absorb preferentially left vs. right circularly polarized light (or vice versa) giving rise to the absorption CD (see image of the helix in *b*). Thus, the final difference in intensity between the two polarizations in the transmitted light will be the result of the superposition of the two mechanisms for energy removal depicted in *a* and *b* and so will be the image of the helix, which will be formed on the screen.

can be obtained by subtracting the CD^{sca} from the CD^{obs} image of the object. To avoid significant differences in resolution between the two images, and to minimize the wavelength dependence of the scattering contributions, it is convenient to choose the wavelengths, λ_{in} and λ_{out}, as close as possible.

In mathematical form, the expression that controls the magnitude and sign of the CD^{obs} image is given by (see accompanying paper [4b]):

$$CD^{obs} = -\left\{4\pi k^2 AB\left[\sum_{i}^{N}\sum_{j\neq i}^{N}\frac{J_1\left(\frac{ka\rho_i}{r}\right)}{\frac{ka\rho_i}{r}} \cdot \alpha_i^*\alpha_j^* e^{-i\mathbf{k}_o\cdot\mathbf{r}_{ij}}(\hat{\mathbf{t}}_j\cdot\mathbf{\Gamma}_{ji}^*\cdot\hat{\mathbf{t}}_i)H + \sum_{i}^{N}\sum_{j\neq i}^{N}\frac{\mathbf{J}_1\left(\frac{ka\rho_i}{r}\right)}{\frac{ka\rho_i}{\mathbf{r}}} \cdot \alpha_i\alpha_j e^{i\mathbf{k}_o\cdot\mathbf{r}_{ij}}(\hat{\mathbf{t}}_i\cdot\mathbf{\Gamma}_{ij}\cdot\hat{\mathbf{t}}_j)H\right]\right\}, \qquad (5)$$

where $H \equiv (\hat{\mathbf{t}}_i\cdot\hat{\epsilon}_H)(\hat{\epsilon}_H\times\hat{\mathbf{t}}_j)\cdot\hat{\mathbf{z}} + (\hat{\mathbf{t}}_i\cdot\hat{\epsilon}_V)(\hat{\epsilon}_V\times\hat{\mathbf{t}}_j)\cdot\hat{\mathbf{z}}$. Notice that this expression contains only higher Born approximations because the first Born approximation contribution to the CD^{obs} image vanishes, as shown in the previous paper (4b). The polarizability tensor, $\boldsymbol{\alpha}_i$, appearing in Eq. 5 is in general, complex.

Eq. 5 can be further simplified to obtain:

$$CD^{obs} = -8\pi k^2 AB\left[\sum_{i}^{N}\sum_{j\neq i}^{N}\frac{J_1\left(\frac{ka\rho_i}{r}\right)}{\frac{ka\rho_i}{r}} \cdot \mathrm{Re}(\alpha_i\alpha_j\mathbf{T}_{ij}e^{i\mathbf{k}_o\cdot\mathbf{r}_{ij}})H\right], \qquad (6)$$

where $\mathbf{T}_{ij} = \hat{\mathbf{t}}_i\cdot\mathbf{\Gamma}_{ij}\cdot\hat{\mathbf{t}}_j$

In general, the polarizability associated to any group k in the object can be written as $\boldsymbol{\alpha}_k = \boldsymbol{\alpha}'_k + i\boldsymbol{\alpha}''_k$, where $\boldsymbol{\alpha}'_k$ and $\boldsymbol{\alpha}''_k$ are the real and imaginary parts of the polarizability tensor, respectively. Mathematically, the CD^{sca} contribution corresponds to choosing only real and symmetric tensors for the group polarizabilities. Eq. 6 becomes in this case:

$$CD^{sca} = -8\pi k^2 AB\left[\sum_{i}^{N}\sum_{j\neq i}^{N}\frac{J_1\left(\frac{ka\rho_i}{r}\right)}{\frac{ka\rho_i}{r}} \cdot \alpha'_i\alpha'_j\mathrm{Re}(\mathbf{T}_{ij}e^{i\mathbf{k}_o\cdot\mathbf{r}_{ij}})H\right]. \qquad (7)$$

This equation contains only the scattering contribution to the preferential removal of the energy between right and left circularly polarized incident light. If λ_{in} is not too different from λ_{out}, Eq. 7 can be subtracted from Eq. 6 to obtain an expression for CD^{abs}:

$$CD^{abs} = 8\pi ABH\sum_{i}^{N}\sum_{j\neq i}^{N}\frac{J_1\left(\frac{ka\rho_i}{r}\right)}{\frac{ka\rho_i}{r}} \cdot [\alpha''_i\alpha''_j R_e(\mathbf{T}_{ij}e^{i\mathbf{k}_o\cdot\mathbf{r}_{ij}}) + (\alpha''_i\alpha'_j + \alpha'_i\alpha''_j)\mathrm{Im}(\mathbf{T}_{ij}e^{i\mathbf{k}_o\cdot\mathbf{r}_{ij}})]. \qquad (8)$$

Eq. 8 shows that two terms contribute to the magnitude and sign of the CD^{abs} image: one proportional to the interference between the imaginary parts of the polarizabilities of any two groups in the molecule; the other proportional to the interference between the absorptive (imaginary) and refractive (real) properties of the polarizabilities. The former term represents the pure absorptive properties of a chiral object composed of many interactive groups. The magnitude of this term is mainly determined by the chromophore density in the object, and by how well the spatial shape of the electric field of one of the two circular polarizations matches the shape, handedness, and dimensions of the chiral organization in the object (6). The second term in Eq. 8 is likely to be negligible with respect to the first because usually the real part of the polarizability, at the center of the absorption band, is much smaller than its imaginary part.

Eqs. 7 and 8 represent the separated contributions of scattering and absorption to the CD image in bright field geometry. A way to carry out this separation experimentally is by performing separate measurements of CD^{sca} in a scattering experiment that excludes the forward direction.

B. CD^{sca} from M_{14} images taken with lenses of different numerical apertures

The expression of M_{14} in Eq. 6 is a function of the lens radius a or, equivalently, a function of its numerical aperture (N.A.). The smaller the radius, the smaller the acceptance angle θ of the lens, which means that more scattered radiation escapes the lens, contributing to the image through the power loss mechanism explained in the introduction. If images of an object are obtained using two lenses of different size, while the absorption contribution must be the same in both cases, the scattering contribution to the images differs by an amount depending on the difference between the numerical apertures of the lenses. If the M_{14} image obtained with the larger lens (of radius a_2) is subtracted from the M_{14} image formed with the smaller lens (of radius a_1), the absorption contribution and most of the scattering should cancel, leaving only the contribution due to a scattering cone whose basis is the difference between the surfaces of the two lenses $[\pi(a_1)^2 - \pi(a_2)^2]$, and whose vertex is at the object. This is depicted schematically in Fig. 2. To obtain an expression for this scattering contribution, Eq. 2 can be used. The difference between the two images will be:

$$\begin{aligned}\Delta M_{14}(\Delta a) = M_{14}(a_1) - M_{14}(a_2) = \\ -A\frac{r_o^2}{k^3}\{[a_1^{-2}(\mathbf{1} \times \mathbf{F}(a_1)^\dagger - \mathbf{F}(a_1) \times \mathbf{1}) \\ -a_2^{-2}(\mathbf{1} \times \mathbf{F}(a_2)^\dagger - \mathbf{F}(a_2) \times \mathbf{1})] \\ + \mathbf{F}(a_1) \times \mathbf{F}(a_1)^\dagger - \mathbf{F}(a_2) \\ \times \mathbf{F}(a_2)^\dagger\}_{\alpha\beta\gamma}(\mathbf{1} - \hat{\mathbf{z}}\hat{\mathbf{z}})_{\alpha\gamma}\hat{\mathbf{z}}_\beta,\end{aligned} \tag{9}$$

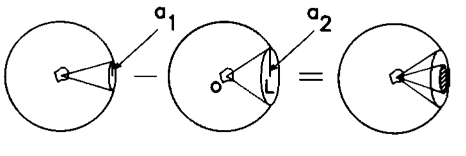

FIGURE 2 The figure shows how the size of a lens (L), and therefore its angle of acceptance and N.A., determine how much of the radiation energy, removed by scattering, will contribute to the CD^{obs}. In the case of the smaller lens (*left*) scattering from the object (o) contributes differently from that of the larger lens (*middle*). The difference between CD^{obs} obtained with the small lens and CD^{obs} obtained with the large lens (*right*) leads to the characterization of the scattering occurring between the angle of acceptance of the two lenses.

where a_1 and a_2 are the radii of the two lenses, and $a_1 < a_2$. The term on the right-hand side of Eq. 9, containing the difference between tensors ($\mathbf{F} \times \mathbf{F}^\dagger$), represents the forward scattering, but is negligible compared to the term in the brackets because it involves the difference between two very small quantities (see previous section). The only surviving term in Eq. 9 is the difference between the extinction contributions. Taking $a_1 = a$ and $a_2 = a + \Delta a$, this term becomes:

$$\begin{aligned}-A\frac{r_o^2}{k^3}\{a^{-2}[\mathbf{F}(a + \Delta a) \times \mathbf{1} - \mathbf{F}(a) \times \mathbf{1}]_{\alpha\beta\gamma} \\ - (a + \Delta a)^{-2}[\mathbf{1} \times \mathbf{F}(a + \Delta a)^\dagger \\ - \mathbf{1} \times \mathbf{F}(a)^\dagger]_{\alpha\beta\gamma}\}(\mathbf{1} - \hat{\mathbf{z}}\hat{\mathbf{z}})_{\alpha\gamma}\hat{\mathbf{z}}_\beta.\end{aligned} \tag{10}$$

Keeping only terms proportional to a^2, in the limit of small Δa's:

$$\Delta M_{14} = -A\frac{r_o^2}{k^3}\frac{\Delta a}{a^2}\left[\frac{\partial \mathbf{F}(a)}{\partial a} \times \mathbf{1} - \mathbf{1} \times \frac{\partial \mathbf{F}(a)^\dagger}{\partial a}\right]_{\alpha\beta\gamma}(\mathbf{1} - \hat{\mathbf{z}}\hat{\mathbf{z}})_{\alpha\gamma}\hat{\mathbf{z}}_\beta. \tag{11}$$

Carrying out the differentiation, this equation becomes:

$$\Delta M_{14} = -A\frac{r_o^2}{k^3}\frac{\Delta a}{a^3}\sum_i^N\left\{\left[\frac{x_i J_o(x_i) - 2J_1(x_i)}{x_i}\right] \cdot [\boldsymbol{\alpha}_i \times \mathbf{1} - \mathbf{1} \times \boldsymbol{\alpha}_i^\dagger]_{\alpha\beta\gamma}(\mathbf{1} - \hat{\mathbf{z}}\hat{\mathbf{z}})_{\alpha\gamma}\hat{\mathbf{z}}_\beta\right\}, \tag{12}$$

where

$$x_i = \frac{ka\rho_i}{r}.$$

This expression contains the dependence of ΔM_{14} on the lens radius and gives the preferential scattering contribution to the CD image in the cone spanned between the scattering angle θ and $\theta + \Delta\theta$. In our notation (consistent with that used in the first paper in this series [5]), the angle θ is defined in terms of the lens radius as: $\theta \equiv$

$\tan^{-1}(a/x_0)$, where x_0 is the distance between the object and the lens (refer to Fig. 1 of paper I for details [5]). Eq. 12 can be used for all orders in the Born expansion, as long as the α's are chosen appropriately.

III. CALCULATIONS

Calculations have been carried out to model the results obtained in section II A and B. All the calculations were performed using right-handed helices immersed in a medium with index of refraction $n = 1.5$. The model helices have three turns with 10 equally spaced groups per turn. The polarizability tensor of each group is assumed to be uniaxial and this axis is oriented tangentially to the line of the helix. Also, the helix axis is perpendicular to the direction of propagation of the light. In all cases the second Born approximation was used and the image calculated was normalized with respect to the unpolarized image (M_{11} entry of the Mueller matrix).

A. Separation of CD^{sca} and CD^{abs} contributions to the M_{14} image

M_{14} images inside (CD^{obs}) and outside (CD^{sca}) the absorption band have been computed for two helices with dimensions smaller and larger than the wavelength of the light. One helix has pitch = 100 λ and radius = 50 λ, whereas the other has pitch = 0.1 λ and radius = 0.05 λ. For each helix CD^{obs} was calculated choosing complex polarizability tensors, according to Eq. 6, whereas CD^{sca} was calculated using real polarizability tensors, according to Eq. 7. Then, the normalized CD^{sca} image was subtracted from the normalized CD^{obs} image to obtain the CD^{abs} image. All the calculations are displayed as contour plots. Each contour line connects points of equal intensity of the differential ratio M_{14}/M_{11}. Dashed lines indicate negative values, while solid lines indicate positive values of the differential ratio. All the images are also thresholded to eliminate values smaller than one hundredth the maximum positive and negative dichroic ratio.

Fig. 3, *a* and *b*, show the CD^{obs} and the CD^{sca} of the larger helix, respectively; the lens radius was kept constant for these two calculations at 10,000 λ. Fig. 3 *c* displays the difference between the images in Fig. 3, *a* and *b*. Given the nature of the contour plotting routine, only some of the differential values calculated are represented in the figure, however, after integrating the CD values of opposite sign over the whole helix, it was found that these three images are dominated by positive values. This indicates that a right-handed helix of these dimensions, and orientation absorbs and scatters preferentially left versus right circularly polarized light. Note that the sum of the positive integrated values of the dichroic ratio in CD^{abs} and CD^{sca} equals the average positive value in the CD^{obs} image (see figure caption). Similarly, the sum of the negative integrated values of the dichroic ratio in CD^{abs} and CD^{sca} equals the inte-

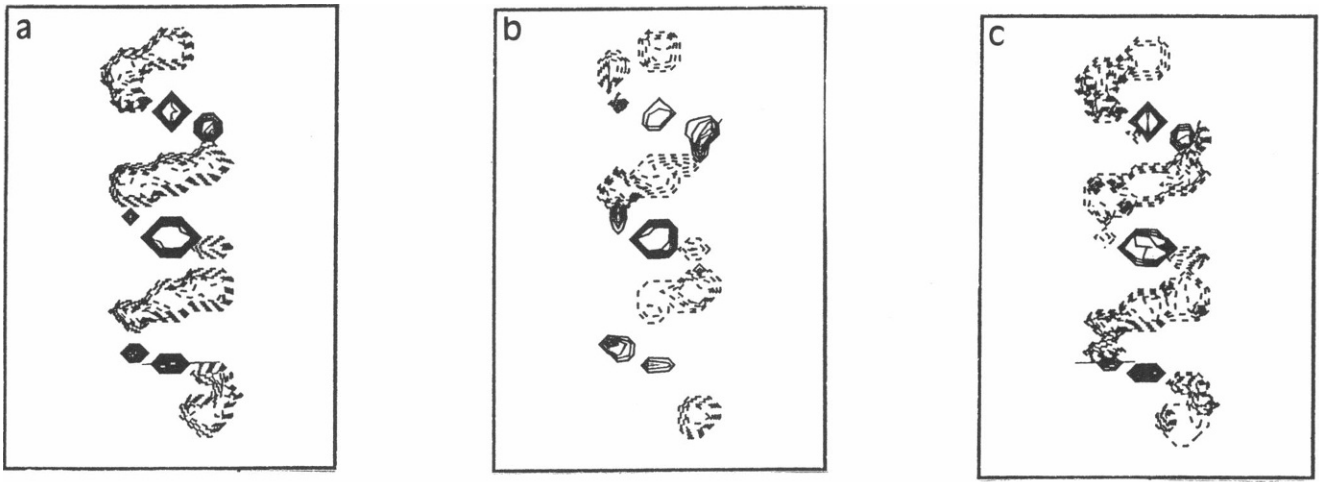

FIGURE 3 Right-handed helix having pitch = 100 λ, radius = 50 λ. The helix has three turns, 10 groups per turn at 36° with respect to each other. The distance of the helix to the lens is 6666.7 λ, that between the lens and the detector screen is also 6666.7 λ, while the focal length is 3333.3 λ. Data are calculated every 8.3 λ (*a*) normalized CD^{obs} image. The polarizability tensors are complex. The lens radius is 10,000 λ. The integrated intensities of the positive and negative values are 0.813, and −0.592, respectively. (*b*) Normalized CD^{sca} image. The polarizability tensors are real. The lens radius is 10,000 λ. The integrated intensities of the positive and negative values are 0.367 and −0.316, respectively. (*c*) CD^{abs} obtained by subtracting CD^{sca} from CD^{obs}. The integrated intensity of the positive values is 0.465, that of the negative values is −0.403.

grated negative value of the dichroic ratio in CD^{obs}. Integration of the differential ratio values displays the additivity of the adsorption and scattering contributions in the observed signal. In fact, comparison of local differential ratio values may be misleading because absorption and scattering domains may not necessarily coincide. Finally, it should be noticed how these three M_{14} images show the dependence of optical activity on the orientation of the individual groups. The effect of the orientation determines the sign of the alternating stretches in the helix image and also whether the image is built up of individual domains or is more continuous.

The CD^{obs}, CD^{sca}, and CD^{abs} for a right-handed helix whose dimensions are one order of magnitude smaller than those of the wavelength of light, are shown in Fig. 4, *a–c*, respectively. In this case, both CD^{obs} and CD^{sca} are dominated by positive values of the dichroic ratio, whereas in CD^{abs} the negative values are dominant. In this case, both CD^{obs} and CD^{sca} are dominated by positive values of the differential ratio, whereas in CD^{abs} the negative values are dominant. Notice, that even though Fig. 4, *a*and *b*, look identical the intensity of the differential ratio values in Fig. 4 *a* is four orders of magnitude smaller than that in Fig. 4 *b* (see figure caption). Also, because CD^{abs} and CD^{sca} are spatially similar, but opposite in sign, the sum image (CD^{obs}) is not "deformed" and has the appearance of CD^{sca}, even if the overall optical activity is diminished due to cancellation effects. Thus, a right-handed helix of these dimensions, and orientation absorbs more right, but scatters more left circularly polarized light. The cancellation of the CD^{abs} and CD^{sca} shows up in the smaller magnitude of the integrated values of the CD^{obs} image. From the values of CD^{sca} it is seen that this helix does not scatter differentially as much as the bigger helix in Fig. 3. As mentioned in section II A, the chiral dimensions of the object and the distance between polarizable groups affect the amount of preferential scattering. Whereas for the large helix of Fig. 3 the distance between adjacent polarizable groups in the object is 3.3 λ, in this helix this distance is 0.0033 λ. This explains why the differential ratio values in Fig. 4, *a* and *b*, are smaller than in Fig. 3, *a* and *b*. For the same reason, the orientational dependence of the optical activity is not as marked as in Fig. 3.

B. Effect of the numerical aperture on the M_{14} image

It has been shown in section II B that decreasing the radius of the imaging lens changes the contribution of the apparent CD to the M_{14} image. In fact, varying the N.A. of the lens corresponds to increasing or decreasing the acceptance angle of the lens, allowing a bigger or smaller number of scattering lobes likely of different sign and magnitude, to contribute to the signal observed in the forward direction (CD^{obs}). Thus, if a CD^{obs} image obtained with a large aperture lens is subtracted from a CD^{obs} image obtained with a lens of smaller aperture, the absorption and most of the scattering contributions

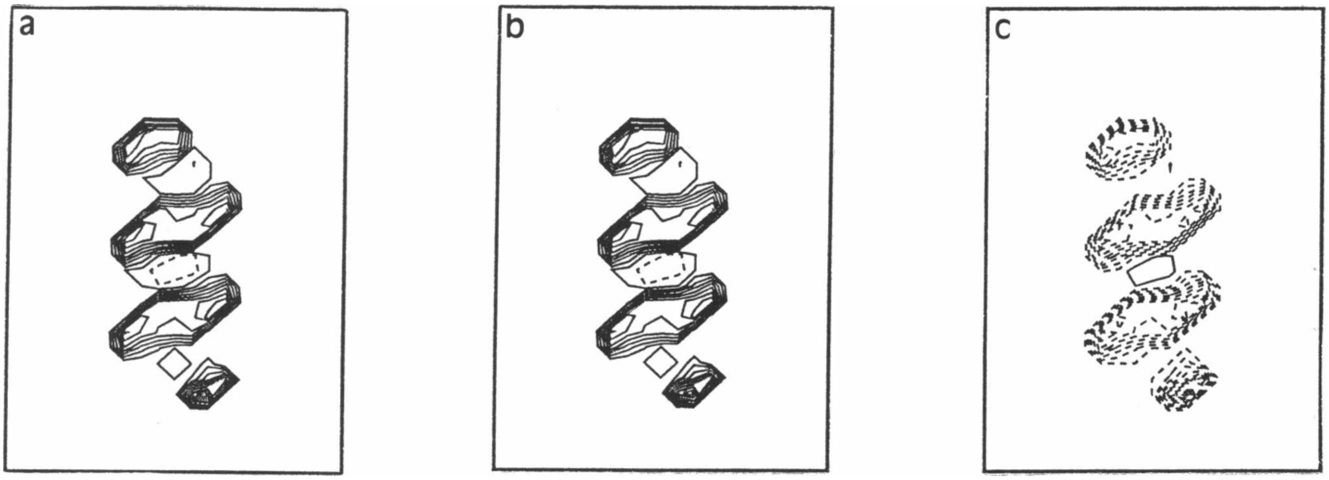

FIGURE 4 Right-handed helix having pitch = 0.1 λ, radius = 0.05 λ. This helix also has three turns, ten groups per turn at 36°. The distance of the helix to the lens is 66.7 λ, that between the lens and the detector screen is also 66.7 λ, whereas the focal length is 33.3 λ. Data are calculated every 0.02 λ (*a*) normalized CD^{obs} image. The polarizability tensors are complex. The lens radius is 500 λ. The integrated intensities of positive and negative values are 1.0E-5; −1.8E-6. (*b*) Normalized CD^{sca} image. The polarizability tensors are real. The lens radius is 500 λ. The integrated intensities of positive and negative values are 0.103; −0.018. (*c*) CD^{abs} obtained by subtracting CD^{sca} from CD^{obs}. The integrated intensity of positive and negative values in this image are 0.016; −0.103.

will cancel, except for the preferential scattering in the conical region delimited by the acceptance angles of the two lenses. This procedure provides a way to characterize the differential scattering contribution to the CD images of specific scattering angles in space. Calculations were performed using a right-handed helix with pitch of 10 λ and radius of 5 λ. Fig. 5 *a* shows the M_{14} image of the helix calculated using a lens radius = 721 λ (N.A. = 1.36, $\theta = 65°$). This image is dominated by positive values of the dichroic range (see figure caption). Fig. 5 *b* shows the M_{14} image of the same helix, calculated using a lens radius = 843 λ (N.A. = 1.39, $\theta = 68°$). This image also is dominated by positive values of the dichroic ratio. The difference image between Fig. 5, *a* and *b*, representing the scattering contribution between 65° and 68°, is shown in Fig. 5 *c*. Here, the negative values prevail indicating that in this particular range of angles the helix scatters, in average, more left than right

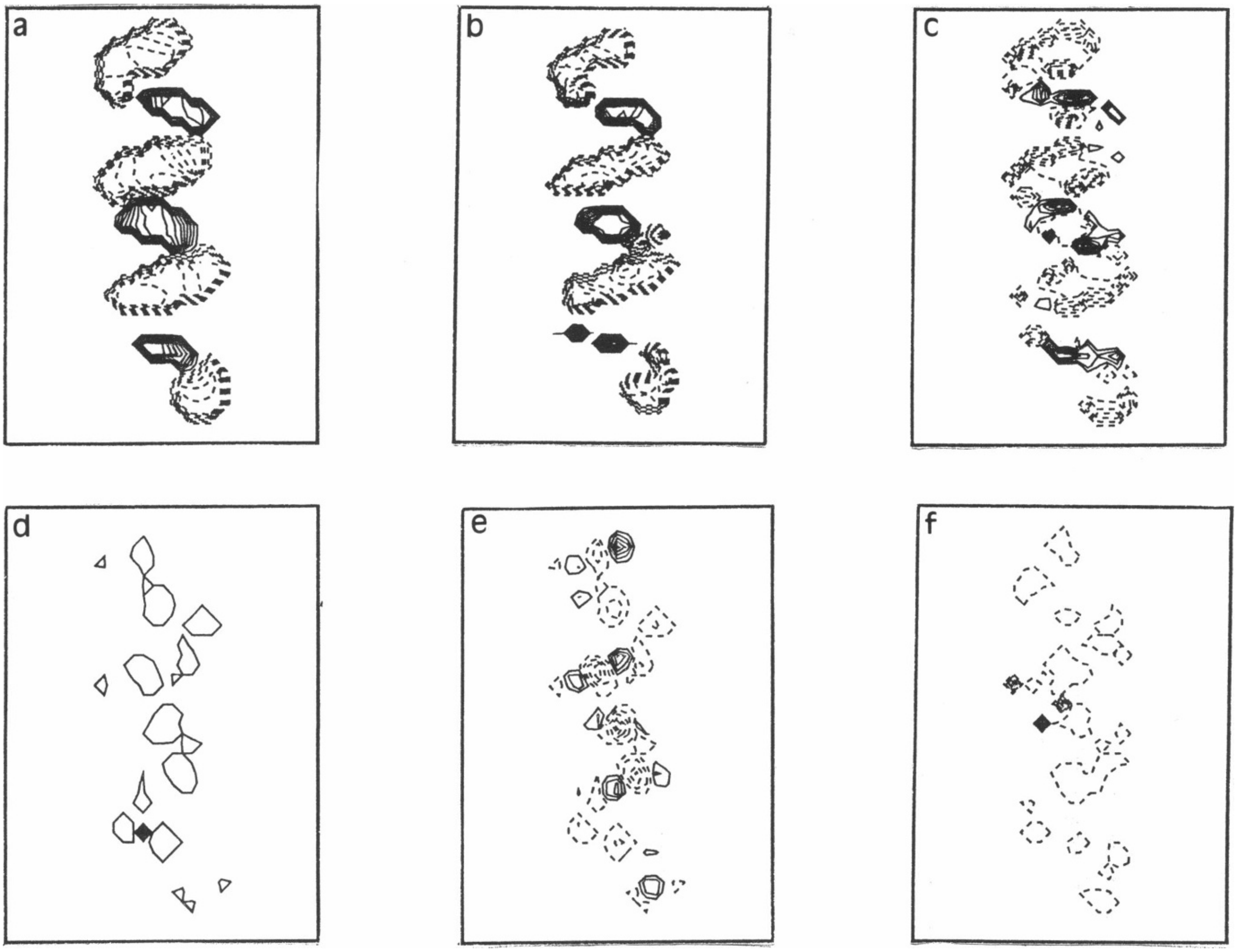

FIGURE 5 Scattering contributions at different angles in space to the M_{14} image of a right-handed helix with pitch 10 λ and radius 5 λ, three turns, 10 groups per turn at 36°. The distance of the helix to the lens is 666.7 λ, that between the lens and the detector screen is also 666.7 λ, whereas the focal length is 333.3 λ. The data are calculated every 0.83 λ. (*a*) CD^{obs} calculated using a N.A. = 1.36, $\theta = 65°$. The integrated positive value is 70.6, whereas the integrated negative value is −58.7. (*b*) CD^{obs} calculated using a N.A. = 1.39, $\theta = 68°$. The integrated positive value is 78.2, whereas the integrated negative value is −60.0. (*c*) CD^{sca} obtained subtracting *b* from *a*. The integrated positive value is 29.6, whereas the integrated negative value is −32.5. (*d*) CD^{sca} contribution to the M_{14} image of this helix occurring between 69.73 and 69.76°. This image was obtained by subtracting the helix M_{14} image obtained with a N.A. = 1.4071 from that obtained with a N.A. = 1.4074. Integrated positive value = 1.1E-3, integrated negative = −6.0E-4. (*e*) Scattering occurring between 69.76 and 69.83°. This image was obtained by subtracting the helix M_{14} image calculated with a N.A. = 1.4074 from that calculated with a N.A. = 1.4079. Integrated positive value = 1.1E-3, integrated negative value = −1.1E-3. (*f*) Scattering occurring between 69.83 and 69.97°. This image was obtained by subtracting the helix M_{14} image calculated with N.A. = 1.4079 from that calculated with N.A. = 1.409. Integrated positive value = 1.2E-2, integrated negative value = −1.9E-2.

circularly polarized light. M_{14} images of the same right-handed helix were calculated also using lenses of radii equal to 903 λ, (N.A. = 1.4071, θ = 69.73°), 904 λ, (N.A. = 1.4074, θ = 69.76°), 907 λ (N.A. = 1.4079, θ = 69.83°), 914 λ (N.A. = 1.409, θ = 69.97°), which represent smaller increments in the angle of acceptance. Fig. 5 *d* shows the difference between the first two images and it represents the scattering between 69.73 and 69.76°. From the values of the differential ratio, it can be seen that the positive integrated differential value is larger than the negative integrated value by an order of magnitude (see figure caption), indicating that this helix scatters more left than right circularly polarized light in this range of angles. Fig. 5 *e* shows the scattering occurring between 69.76 and 69.83°, whereas Fig. 5 *f* shows the scattering occurring between 69.83 and 69.97°. In Fig. 5 *e* the positive and negative integrated values of the differential ratio are exactly the same, thus, the preferential scattering integrated over the whole helix is zero in this range of angles. This corresponds to a region in space, between two lobes of opposite sign, in which the CIDS vanishes ("node"). On the other hand, Fig. 5 *f* is dominated by negative values of the differential ratio. The three difference images reveal two lobes of preferen-

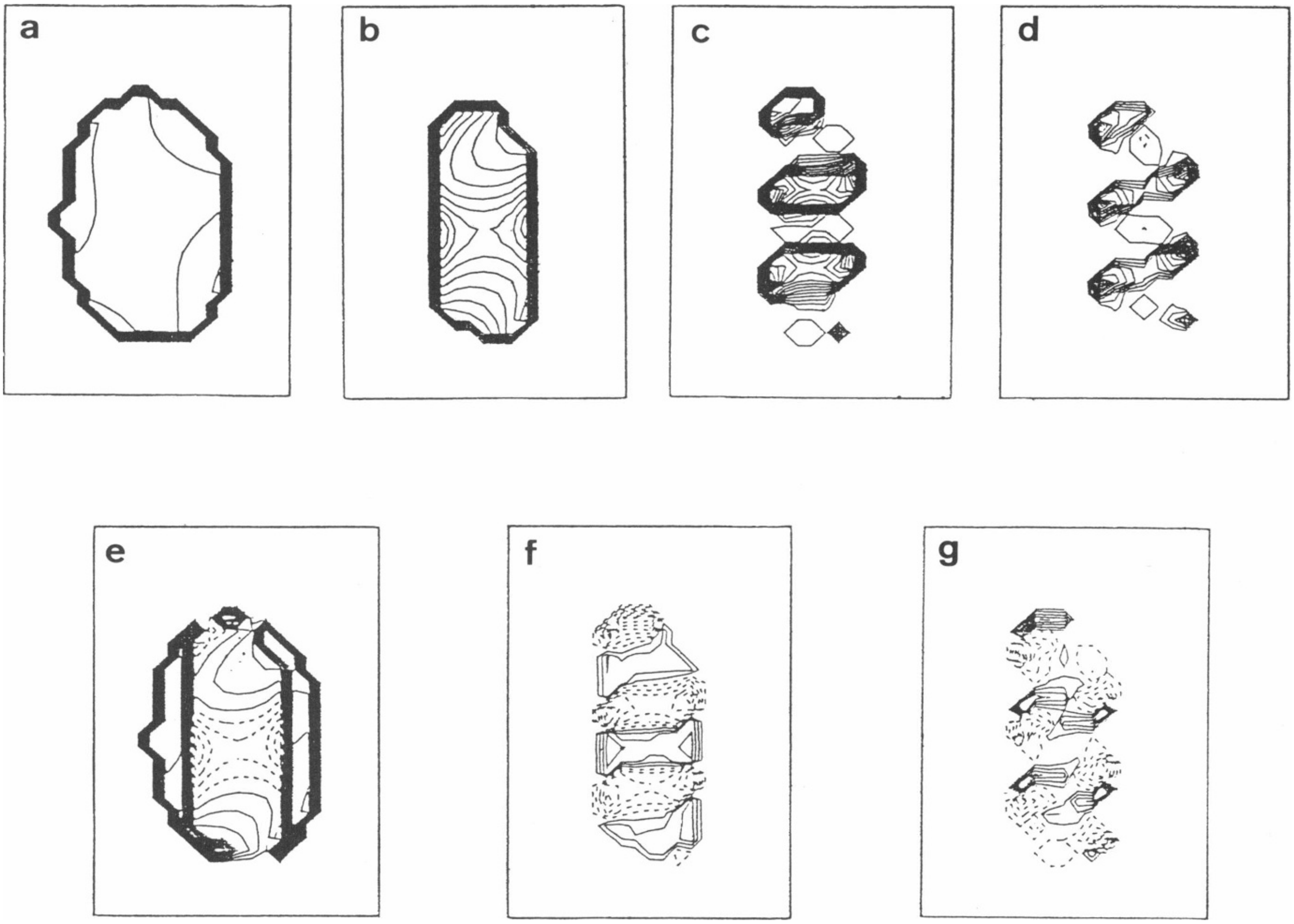

FIGURE 6 Scattering contributions at different angles in space to the M_{14} image of a right-handed helix with pitch 0.6 λ and radius 0.3 λ, three turns, 10 groups per turns at 36°. The distance of the helix from the lens is 416.7 λ, that between the lens and the detector screen is also 416.7 λ, whereas the focal length is 208.3 λ. The data are calculated every 0.1 λ. (*a*) CD^{obs} calculated using a N.A. = 1.46. The integrated positive value is 0.063. (*b*) CD^{obs} calculated using a N.A. = 1.48. The integrated positive value is 0.060. (*c*) CD^{obs} calculated using a N.A. = 1.494. The integrated positive value is 0.092, whereas the integrated negative value is −0.006. (*d*) CD^{obs} calculated using a N.A. = 1.498. The integrated positive value is 0.12, whereas the integrated negative value is −0.017. (*e*) CD^{sca} obtained subtracting *b* from *a*. The integrated positive value is 3.5, whereas the integrated negative value is −0.71. This image represents the scattering between 77 and 82°. (*f*) CD^{sca} contribution to the M_{14} image of this helix occurring between 82 and 84°. Integrated positive value = 5.2, integrated negative = −5.6 (*g*) Scattering occurring between 84 and 87°. Integrated positive value = 5.8, integrated negative value = −4.7.

tial scattering of opposite sign and a zero or node. A helix of these dimensions has eighty scattering lobes and eighty "nodes" over 360° in the scattering plane, containing the incident light and perpendicular to the helix axis (7). Calculations were also performed on a smaller helix of radius 0.3 λ and pitch 0.6 λ. This helix is predicted to have five lobes (7). Fig. 6, *a–d*, show the images of this helix obtained using a lens radius of 890 λ (N.A. = 1.46, $\theta = 77°$), 1550 λ (N.A. = 1.48, $\theta = 82°$), 2360 λ (N.A. = 1.494, $\theta = 84°$), 4760 λ (N.A. = 1.498, $\theta = 88°$), respectively. Fig. 6 *e* shows the difference between the first two images and it represents the scattering between 77 and 82°. From the values of the differential ratio it can be seen that the positive integrated differential value is larger than the negative integrated value by an order of magnitude (see figure caption), indicating that the helix scatters more left than right circularly polarized light in this range of angles. Fig. 6 *f* shows the scattering occurring between 82 and 84°. Here the image is slightly dominated by negative values (see figure caption), indicating that in this region in space, the helix scatters more right than left circularly polarized light. Fig. 6 *g* shows the scattering occurring between 84 and 88°. In this case the positive values of the differential ratio dominate over the negative (see figure caption). These last three difference images reveal three of the five lobes characterizing the scattering pattern of this helix. By calculating more images and determining the average intensity of positive and negative preferential scattering for each calculation, one can have enough points to plot the scattering lobes as function of angle. The contribution of each scattering lobe to the CD^{obs} image of any helix can be obtained and mapped with the method outlined above.

IV. EXPERIMENTAL CONFIRMATION

M_{14} images of chloroplasts were taken using a differential polarization microscope (8) to verify the predictions

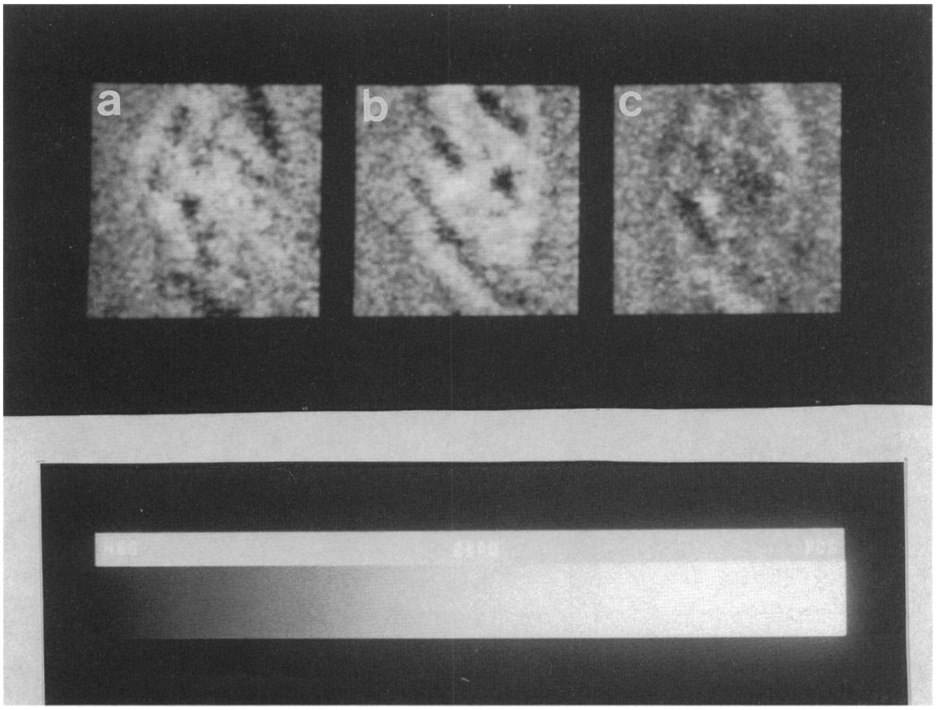

FIGURE 7 Differential polarization M_{14} images of an aligned chloroplast performed with a confocal scanning differential polarization microscope. The grey scale for the dichroic ratio is shown. (*a*) CD^{obs} obtained by using light of wavelength = 515 nm. In this image, the integrated positive and negative values of the dichroic ratio were +5.8E-4 and −4.8E-4, respectively. The extremes of the grey scale correspond, in this image, to a dichroic ratio of +/−2.91E-3. (*b*) CD^{sca} obtained by using light of wavelength = 546 nm. The integrated positive and negative values of the dichroic ratio were +6.7E-4 and −6.2E-4, respectively. The extremes of the grey scale correspond, in this image, to a dichroic ratio of +/−1.4E-3. (*c*) Difference image between CD^{sca} and CD^{obs}. CD^{sca} was rescaled to 2.91E-3, before the subtraction was performed. The integrated positive and negative values of the dichroic ratio were +2.93E-4 and −2.96E-4, respectively. The extremes of the grey scale correspond, in this image, to a dichroic ratio of +/−2.91E-3. The size of the images is 6.4 × 6.4 um.

of the theory developed in section II. Chloroplasts are photosynthetic organelles of highly organized molecular structure. The efficiency of the photosynthetic conversion of light energy is largely determined by the organization of the photosynthetic pigment molecules embedded in the membranes contained in chloroplasts (9, 10). Several levels of chirality in chloroplasts have been suggested by CD studies of chloroplast suspensions (4) as well as in CIDS studies of chloroplast suspensions (11). Cloroplasts are, therefore, both absorbing and scattering systems. The CIDS signals indicate that at 515 nm (one of the absorption bands of chloroplasts), there is considerable preferential scattering by long-range, left-handed chiral structures with dimensions close to 400 nm. Such macroorganization can play an important role in energy transfer to the reaction center. This suggests that the M_{14} images recently obtained using light inside the absorption band, by means of differential polarization microscopy (4), contain absorption (CD^{abs}) as well as scattering (CD^{sca}) contributions.

The only way to separate experimentally the CD^{sca} from the CD^{abs} contribution is to measure CD^{sca} independently, in a scattering experiment that excludes the transmitted beam. Nonetheless, M_{14} images of chloroplasts obtained inside and outside the absorption band of the chromophores will be shown here to illustrate the sensitivity of the CD image to the wavelengths dependence of the scattering and absorption contributions. Images of chloroplasts were taken at 515 and 546 nm. 515 nm is the peak of absorption of chloroplasts in the green region of the visible spectrum, whereas 546 nm is outside the absorption band. All the chloroplasts examined were magnetically aligned to simplify the interpretation and reproducibility of the data (4). The CD^{obs} of an aligned chloroplast at 515 nm is shown in Fig. 7 *a* and the CD^{sca} at 546 nm in Fig. 7 *b*. Fig. 7 *c* represents the difference between Fig. 7 *a* and *b* pixel by pixel. All the differential images are shown in a gray scale where white and lighter grays encode positive values of the differential ratio, gray indicates a zero value, and darker grays and black encode negative values of the differential ratio. CD^{obs} and CD^{sca} are dominated by positive values (see figure caption), in agreement with the positive band and tail observed in the green region of the macroscopic spectrum of aligned chloroplast suspensions (12). The difference image shown in Fig. 7 *c* is of more difficult interpretation because the absorption band is broad and the wavelengths chosen to record CD^{obs} and CD^{sca} are several nanometers apart. Because of this, the scattering contributions in these two images are not the same and therefore do not subtract out when taking the difference. Even though Fig. 7 *c* cannot be interpreted as CD^{abs}, it is interesting to notice that the integrated positive and negative values of the dichroic ratio are almost equivalent, although the negative values slightly dominate. The weakness of the signals in Fig. 7 *c* indicates that in this case, the scattering at 546 nm cancels out most of the signals obtained at 515 nm, suggesting that scattering is a big part of CD^{obs} at 515 nm, in agreement with what has been suggested by Garab et al. (13).

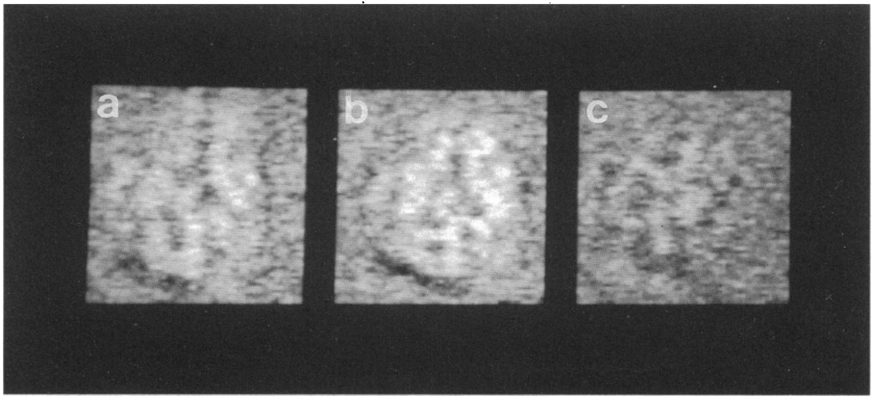

FIGURE 8 Differential polarization M_{14} images of a chloroplast. (*a*) CD^{obs} obtained at 515 nm with a N.A. = 0.8, corresponding to an angle of acceptance of 36°. The integrated positive and negative values of the dichroic ratio were +3.8E-4 and −3.4E-4, respectively. The extremes of the gray scale correspond for this image, to a dichroic ratio of +/−2.35E-3. (*b*) CD^{obs} obtained at 515 nm with a N.A. = 1.25, corresponding to an angle of acceptance angle of 63°. The integrated positive and negative values of the dichroic ratio were +3.4E-4 and −3.3E-4, respectively. The extremes of the gray scale correspond, for this image, to a dichroic ratio of +2.35E-3. (*c*) Difference between the M_{14} image obtained with a smaller N.A. (*a*) and that obtained with a larger N.A. (*b*). This image represents the scattering contribution to the overall M_{14} image of the chloroplast, occurring between 32 and 56°. The integrated positive and negative values of the dichroic ratio were +2.1E-4 and −2.5E-4, respectively. The extremes of the gray scale correspond, in this image, to +/−2.35E-3. The size of the images is 6.4 um × 6.4 um.

Experimental verification of the dependence of M_{14} on the size of the lens, derived in section II B and calculated in section III B, was also performed. An objective with variable N.A. was used to image chloroplasts. Fig. 8 *a* shows the CD^{obs} image of a chloroplast obtained at 515 nm with a lens with N.A. = 1.25 ($\theta = 56°$, $n = 1.5$), whereas Fig. 8 *b* shows the CD^{obs} image of the same chloroplast obtained with a N.A. = 0.8 ($\theta = 32°$, $n = 1.5$). The difference between these two images is shown in Fig. 8 *c*. This image represents the preferential scattering occurring between 32 and 56°. From the positive and negative integrated values of the dichroic ratio it can be seen that scattering of right circularly polarized light prevails in this range of angles. This finding agrees with CIDS results (11). The difference between the two N.A.'s used in this experiment is not as small as would be desired. Objectives with several calibrated N.A.'s values would be very useful.

V. CONCLUSION

The separability of the absorption and the scattering contributions to the M_{14} image of a chiral object has been shown theoretically. This separation could facilitate the interpretation of any chiral sample and facilitate the assignment of scattering or absorption domains to different regions in the object. A method to characterize the contribution of the preferential scattering at a particular angle in space, to the CD image of a chiral object, has been proposed. These two methods may be very useful in the study of the anisotropy of biological samples for the new information that they offer in terms of structural organization.

This work was supported by grants from the National Institutes of Health (grant #GM-32543), the National Science Foundation (grant #DIR-8820732), the Center for High Technology and Materials (University of New Mexico [UNM]), the Minority Biomedical Research Support (grant #5-S06-RR0139-15), and the Student Research Allocations Committee of the Graduate Student Association (UNM).

Received for publication 25 July 1990 and in final form 17 December 1990.

REFERENCES

1. Bustamante, C., I. Tinoco, Jr., and M. F. Maestre. 1982. Circular intensity differential scattering of light. IV. Randomly oriented particles. *J. Chem. Phys.* 76:3440–3446.

2a. Dorman, B. P., and M. F. Maestre. 1973. Experimental differential light-scattering correction to the CD of macromolecules. *Proc. Natl. Acad. Sci. USA.* 70:255–259.

2b. Dorman, B. P., J. E. Hearst, and M. F. Maestre. 1973. UV absorption and CD measurements on light scattering of biological specimens; fluorescent cell and related large-angle light detected techniques. *Methods Enzymol.* 27D:767–796.

3. Bustamante, C., I. Tinoco, Jr., and M. F. Maestre. 1983. Circular differential scattering can be an important part of the CD of macromolecules. *Proc. Natl. Acad. Sci. USA.* 80:3568–3572.

4a. Finzi, L., C. Bustamante, G. Garab, and C. Juang. 1989. Direct observation of large chiral domains in chloroplast thylakoid membranes by differential polarization microscopy. *Proc. Natl. Acad. Sci. USA.* 86:8748–8752.

4b. Kim, M., and C. Bustamante. 1991. Differential Polarization Imaging. IV. Images in higher Born approximations. *Biophys. J.* 59:1171–1182.

5. Kim, M., D. Keller, and C. Bustamante. 1987. Differential polarization imaging. I. Theory. *Biophys. J.* 52:911–927.

6. Keller, D., and C. Bustamante. 1986. Theory of the interaction of light with large inhomogeneous molecular aggregates. I. Absorption. *J. Chem. Phys.* 84:2961–2971.

7. Bustamante, C., M. F. Maestre, I. Tinoco, Jr. 1980. Circular intensity differential scattering of light by helical structures. II. Applications. *J. Chem. Phys.* 73:6046–6055.

8. Juang, C., L. Finzi, and C. Bustamante. 1988. Design and application of a computer-controlled confocal scanning differential polarization microscope. *Rev. Sci. Instrum.* 59:2399–2408.

9. Breton, J., and A. Vermeglio. 1982. Photosynthesis. Vol. 1. Govendjee, editor. Academic Press, New York. 153–194.

10. Garab, G., T. Szito, and A. Faludi-Daniel. 1987. The Light Reactions. J. Barber, editor. Elsevier Science Publishers B.V. Amsterdam. 305–339.

11. Garab, G., S. Wells, L. Finzi, and C. Bustamante. 1988. Helically organized macroaggregates of pigment-protein complexes in chloroplasts: evidence from circular intensity differential scattering. *Biochemistry.* 27:5839–5843.

12. Garab, G., L. Finzi, and C. Bustamante. 1991. Differential polarization imaging of chloroplasts. Microscopic and macroscopic linear and circular dicroism. *In* Light in Biology and Medicine. Vol. 2. R. H. Douglas, editor. Plenum Publishing Corp., New York. In press.

13. Garab G., R. C. Leegood, D. A. Walker, J. C. Sutherland, and G. Hind. 1988. Reversible changes in macroorganization of the LH-chlorophyll a/b pigment-protein complex detected by CD. *J. Am. Chem. Soc.* 2430–2434.